



UNIVERSITY OF LEEDS

This is a repository copy of *A core-shell $SO_4/Mg-Al-Fe_3O_4$ catalyst for biodiesel production*.

White Rose Research Online URL for this paper:

<http://eprints.whiterose.ac.uk/149830/>

Version: Accepted Version

Article:

Gardy, J orcid.org/0000-0003-1806-4056, Nourafkan, E, Osatiashtiani, A et al. (4 more authors) (2019) A core-shell $SO_4/Mg-Al-Fe_3O_4$ catalyst for biodiesel production. *Applied Catalysis B: Environmental*, 259. 118093. ISSN 0926-3373

<https://doi.org/10.1016/j.apcatb.2019.118093>

© 2019, Elsevier. This manuscript version is made available under the CC-BY-NC-ND 4.0 license <http://creativecommons.org/licenses/by-nc-nd/4.0/>.

Reuse

This article is distributed under the terms of the Creative Commons Attribution-NonCommercial-NoDerivs (CC BY-NC-ND) licence. This licence only allows you to download this work and share it with others as long as you credit the authors, but you can't change the article in any way or use it commercially. More information and the full terms of the licence here: <https://creativecommons.org/licenses/>

Takedown

If you consider content in White Rose Research Online to be in breach of UK law, please notify us by emailing eprints@whiterose.ac.uk including the URL of the record and the reason for the withdrawal request.



eprints@whiterose.ac.uk
<https://eprints.whiterose.ac.uk/>

A core-shell SO₄/Mg-Al-Fe₃O₄ catalyst for biodiesel production

Jabbar Gardy¹, Ehsan Nourafkan², Amin Osatiashtiani³,

Adam F. Lee⁴, Karen Wilson⁴, Ali Hassanpour^{1, ‡}, Xiaojun Lai^{1, ‡}

¹ School of Chemical and Process Engineering, University of Leeds, West Yorkshire, Leeds, LS2 9JT, UK.

² School of Mathematics and Physics, University of Lincoln, Lincolnshire, Lincoln, LN6 7TS, UK.

³ European Bioenergy Research Institute, Aston University, Aston Triangle, Birmingham, B4 7ET, UK

⁴ Applied Chemistry and Environmental Science, RMIT University, Melbourne, VIC 3000, Australia

‡☎: +44(0) 113 343 2439; ✉ (X.L.): X.Lai@leeds.ac.uk; (A.H.): A.Hassanpour@leeds.ac.uk

Abstract

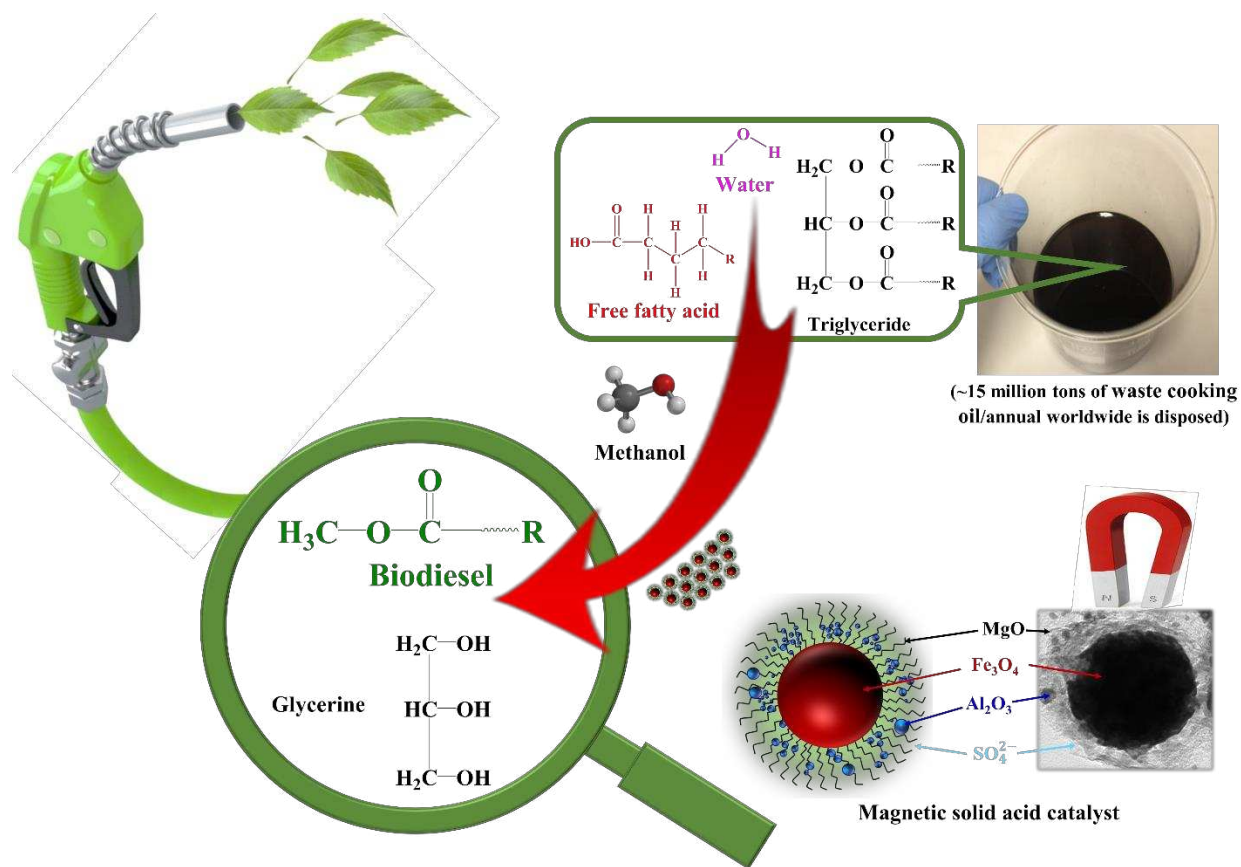
Catalytic transesterification of triglycerides and esterification of free fatty acids underpins sustainable biodiesel production, wherein efficient heterogeneous catalysts are sought to replace mineral acids. A robust, magnetic core-shell SO₄/Mg-Al-Fe₃O₄ catalyst was synthesised by stepwise co-precipitation, encapsulation, and surface functionalisation. The resulting magnetically-separable catalyst has a surface area of 123 m² g⁻¹, uniform 6.5 nm mesopores, and a high total acid site loading of 2.35 mmol g⁻¹. Optimum conditions for the (trans)esterification of waste cooking oil (WCO) over the sulfated solid acid catalyst were 95 °C, a methanol:WCO molar ratio of 9:1, and 300 min reaction to achieve 98.5 % FAME yield. Esterification of oleic acid to methyl oleate resulted in an 88 % yield after 150 min under the same reaction conditions. The magnetic solid acid catalyst exhibited good thermal and chemical stability and enabled facile catalyst separation post-reaction and the production of high quality biodiesel.

Keywords

Solid acid catalyst; magnetic catalyst; core-shell nanoparticle; waste cooking oil; biodiesel

28 **Graphical abstract**

29



30

31

32 **Research highlights**

33

1. A novel magnetic solid acid catalyst was synthesised and characterised.

34

2. The catalyst was active for the (trans)esterification of WCO and oleic acid esterification.

35

3. Efficient biodiesel production from WCO is demonstrated at a low methanol:oil ratio and mild temperature.

36

37

4. Excellent catalytic stability was observed over multiple recycles.

38 **1. Introduction**

39 Energy is a key driving force for transportation, technological advancement, and industrialisation and
40 underpins global socioeconomic development [1-3]. Biodiesel, comprising fatty acid methyl esters
41 (FAME), is widely recognised as a potential low carbon alternative to fossil fuel derived diesel [4], owing
42 to its low toxicity, eco-friendliness [5, 6] and sourcing from non-edible plant and algal oils and animal
43 fats [7-9]. Oils from (micro)algae, jatropha seeds, and waste cooking oil (WCO) feedstocks have been
44 used to reduce biodiesel production costs [9-14]. For example, the amount of WCO generated in the United
45 Kingdom is estimated at 65,000 to 80,000 tons per annum while in China this figure reaches 1,000,000 to
46 2,500,000 per annum from commercial and food processing industries [15]. Such sources could provide
47 an economic alternative to virgin plant oils for biodiesel production, and valorise an otherwise problematic
48 waste stream [2]. However, untreated WCO contains high amounts of free fatty acids (FFAs) and water
49 which renders it an unsuitable feedstock for homogenous base catalysed transesterification with alkaline
50 hydroxides and methoxides due to catalyst neutralisation, hydrolysis of the FAME product, and
51 saponification and attendant separation issues due to the formation of stable emulsions. Homogeneous
52 (acid or base) catalysts also generate large quantities of contaminated wastewater during biodiesel
53 neutralisation [13, 16-19], and essential processing step to avoid engine corrosion.

54 Solid acids and bases can offer good catalytic activity under mild conditions for the (trans)esterification
55 processes of WCO feedstocks [18], and enable efficient product separation and catalyst recycling, in
56 addition to continuous biodiesel production [20]. Although base catalysts are generally more active for
57 triacylglyceride (TAG) transesterification, their sensitivity to FFA contaminants (and necessity for
58 feedstock pre-treatment to remove such impurities) remain problematic [21]. Solid acid catalysts are more
59 resistant to high FFA concentrations, and can simultaneously transesterify TAGs and esterify FFAs to
60 biodiesel [22, 23]. The catalytic activity of solid acids is strongly dependent on the accessibility of bulky
61 reactants to active sites, and the number, strength, and type (Brønsted and/or Lewis) of active site.
62 Numerous solid acids have been explored for biodiesel production, including zeolites, metal oxides and
63 mixed metal oxides, supported acids, polyoxometallates, sulfonated carbons, cation exchange resins and
64 sulfated metal oxides [13, 18, 21, 24-26]. Sulfated metal oxides have attracted significant interest in
65 catalysis [23, 27-32], and are typically synthesised by the preparation of metal oxide sol gel (step 1), the
66 subsequent introduction of sulfate ions by exposure of the sol gel to sulfuric acid [H₂SO₄], chlorosulfonic
67 acid [HSO₃Cl], or ammonium sulfate [(NH₄)₂SO₄] (step 2), and a final calcination at high temperature

68 (step 3). The resulting solid superacidic features SO_4^{2-} groups at the surface on non-porous metal oxide
69 nanoparticles. The acidity of sulfated metal oxides depend on the degree of hydration, preparation method
70 and calcination temperature of the sulfated metal oxide, and the sulfate concentration and presence of
71 neighbouring strong Lewis acid sites [33, 34]. Low sulfate loadings promote bidentate adsorption
72 geometries, whereas high loadings favour Brønsted acidic polynuclear (pyro)sulfates [35, 36]. Sulfated
73 metal oxides, binary metal oxides, and ternary metal oxides are all reported as promising solid acid
74 catalysts for biodiesel production from low cost feedstocks in the presence of FFAs, water, and other
75 impurities. Studies from several authors [37-43] showed that the catalytic activity of sulphated metal
76 oxides could be improved by their fast separation from the product and by-products. The magnetic catalyst
77 has the potential to overcome the limitation for separating solid acid catalysts from the reaction medium.
78 Furthermore, the acidity of magnetic solid acid catalyst reported to be stronger ($H_0 < -13.8$) than 100%
79 sulfuric acid ($H_0 = -12$). For example, the uniform and monodispersed iron oxide nanoparticles were
80 designed by co-precipitation method followed by growing zirconia on the surface of iron oxide
81 nanoparticles whilst the introduction of boron oxide into the solution was to inhibit the nucleation and
82 grain growth of zirconia by delaying the phase transformation of zirconia from tetragonal to monoclinic.
83 The catalytic activity was tested at different calcination temperatures (400-900 °C) for esterifying acetic
84 acid with n-butanol. A yield of $97 \pm 1\%$ was reported under optimum conditions of 4 h, 100 °C, 850 RPM,
85 and 1 atm nitrogen pressure [39]. Another recent study by Wu and co-workers [38] reports the design of
86 a super paramagnetic polysulphated ternary metal oxides catalyst for the transesterification of cottonseeds
87 with methyl acetate. The core was made from iron oxide and prepared by co-precipitation method. Titania
88 and zirconia was introduced to the iron oxide core by another co-precipitation with different mole ratios
89 of Zr/Ti/Fe, followed by impregnation of sulphate ions from $(\text{NH}_4)_2\text{S}_2\text{O}_8$. The final gel was calcined at
90 550, 650 and 750 °C for 3 h. The synthesised magnetic catalysts showed super acidity ($155.3 \pm 0.9 -$
91 $598.6 \pm 1.3 \mu\text{mol/g}$) with polysulphate ions coordinated to $\text{ZrO}_2\text{-TiO}_2\text{-Fe}_3\text{O}_4$ catalyst support. It was
92 reported that $\text{SO}_4/\text{ZrO}_2\text{-TiO}_2\text{-Fe}_3\text{O}_4$ catalyst calcined at 550 °C enabling a FAME yield of 99% after 10.8
93 h at 50 °C with 21.3 wt% of catalyst and 13.8 ml of methyl acetate per g of seed. The acidity of the catalyst
94 increased with the addition of an appreciable amount of titania (3:1 mole ratio of Zr:Ti) into the catalyst
95 texture due to the formation of Zr-O-Ti units during the calcination. This resulted in more sulphur species
96 being adsorbed on the surface and inhibit the zirconia grain growth. As a result, the number of Lewis acid
97 sites increased which enhanced the catalytic activity of the catalyst. The catalyst was re-used for 8 cycles
98 with a slight decrease in activity. Alhassan et al. [37] have also designed a bifunctional magnetic sulphated

99 ternary metal oxide [Fe₂O₃-MnO-SO₄/ZrO₂] catalyst via impregnation method followed by calcination at
100 600 °C for 3 h. This magnetic catalyst was tested for transesterification of WCO under optimum conditions
101 of 180 °C reaction temperature, 20:1 mole ratio of methanol to oil, 3 wt% of catalyst loading, and 600
102 RPM stirring rate, where 97 ± 0.5 % of FAME yield was obtained. The loss of catalytic activity reported
103 after 6 re-runs of the spent catalyst because of pore blockage and sulphur leaching. In summary, the
104 catalytic activity of sulphated metal oxide depends mainly on the precursors, type of sulfonating agent,
105 calcination temperature, amount of sulphate content, and crystallinity of the catalyst. However, there are
106 still prone to deactivation, active site leaching, mass transport limitations, low activity at lower
107 temperatures, water sensitivity, low surface area, and difficult and/or time-consuming separation by
108 filtration or centrifugation [10, 38, 44-49]. These drawbacks highlight the continuing need to design
109 improved catalysts for esterification and transesterification of WCO. Here we report the preparation of a
110 magnetic core-shell SO₄/Mg-Al-Fe₃O₄ nanoparticle catalyst for the simultaneous esterification and
111 transesterification of WCO with methanol under mild conditions. The Fe₃O₄ core facilitates magnetic
112 separation of the solid acid catalyst from the reaction media, while the encapsulating MgAlO_x shell
113 protects the magnetic core and increases the nanoparticle surface area prior to sulfation conferring good
114 activity and stability for biodiesel production even in the presence of high FFA concentrations.

115 **2. Experimental**

116 **2.1 Synthesis of magnetic core-shell SO₄/Mg-Al-Fe₃O₄ catalyst**

117 Iron oxide nanoparticles were synthesised by co-precipitation ($\text{Fe}^{2+} + 2 \text{Fe}^{3+} + 8 \text{OH}^- \rightarrow \text{Fe}_3\text{O}_4 + 4 \text{H}_2\text{O}$).
118 0.2 mol FeCl₂.4H₂O, (≥99.99 %, Sigma-Aldrich) and 0.68 mol FeCl₃.6H₂O (≥98 %, Sigma-Aldrich) were
119 separately dissolved in 25 ml of an aqueous 1:1 vol% ethanol (≥99.8 %, Sigma-Aldrich) solution using an
120 ultrasonic probe. The resulting clear solutions were added to a 250 ml round-bottomed flask, and the
121 solution pH held at 12 by dropwise addition of NH₄OH (28-30 vol%, Sigma-Aldrich), prior to heating at
122 80 °C during stirring (250 rpm) for 6 h under a N₂ atmosphere. Following 24 ageing at room temperature,
123 iron oxide nanoparticles were isolated using an external magnetic field (Nd magnet), and repeatedly rinsed
124 with 1:1 vol% aqueous ethanol until chloride ions could not be detected in the washings. The resulting
125 dark-reddish particles were dried in an oven at 120 °C overnight, and then calcined at 550 °C for 3 h to
126 obtain Fe₃O₄ nanoparticles.

127 Magnesium oxide and alumina encapsulated Fe₃O₄ nanoparticles were synthesised as follows: 3 g of as-
128 prepared Fe₃O₄ nanoparticles were dispersed in 50 ml of 1:1 vol% aqueous isopropanol (+99.5 %, Sigma-
129 Aldrich) using an ultrasonic probe. Subsequently, 50 ml of 1:1 vol% aqueous IPA, 0.6 mol Al(O-i-Pr)₃
130 (+98 % granular, Alfa Aesar) and 0.25 mol Mg(NO₃)₂.6H₂O (≥99.9 %, Sigma-Aldrich) were added
131 dropwise to the mixture along with 1.5 ml of HNO₃ (≥90.0 %, Sigma-Aldrich). The resulting solution was
132 mixed at room temperature for 30 min, and the pH then adjusted to 7 using NH₄OH. This slurry was held
133 at 65 °C during stirring at 250 rpm for 4 h, and then aged at room temperature overnight, and the
134 encapsulated MgO@Al₂O₃@Fe₃O₄ particles magnetically separated, washed with deionised water until
135 pH neutral, and then dried in an oven at 80 °C for 6 h before a final calcined at 550 °C for 2 h. The
136 preceding nanoparticles were functionalised by sulfation. 1.0 g of as-prepared MgO@Al₂O₃@Fe₃O₄
137 nanoparticles was added to 10 ml of 0.5 M (NH₄)₂SO₄ (≥99.5 %, VWR International Ltd) aqueous
138 solution and stirred for 6 h at room temperature. The sulfated nanoparticles were magnetically separated,
139 dried in an oven at 80 °C for 6 h, and finally calcined at 500 °C for 3 h in static air. This sample is denoted
140 SO₄/Mg-Al-Fe₃O₄.

141

142 **2.2 Catalyst characterisation**

143 Powder XRD patterns were measured using a Bruker D8 diffractometer with Cu K_α (λ=1.5418 Å)
144 radiation and a LynxEye detector between 10-70° with steps of 0.035° at 5 s per step. Particle morphology,
145 and elemental composition and spatial distributions were determined using a Hitachi SU8230 cold field
146 emission scanning electron microscope (SEM) operated at 2 kV, and FEI Titan Themis Cubed 300
147 transmission electron microscope (TEM) coupled with an Oxford INCA energy dispersive X-ray
148 spectrometer (EDS). For the TEM analysis magnetic nanoparticles were dispersed in acetone and then drop
149 cast on a carbon coated copper grid. Surface functional groups were examined at room temperature using
150 a Nicolet iS10 FTIR spectrometer by attenuated total reflectance (ATR) between 550-4000 cm⁻¹ at a
151 resolution of 4 cm⁻¹. Textural properties were obtained by N₂ physisorption method at 77 K using a
152 Micromeritics TriStar 3000 porosimeter. The as-prepared magnetic catalyst was degassed in vacuo at 120
153 °C for 16 h prior to analysis, and the surface area calculated using the Brunauer–Emmett–Teller (BET)
154 method over the relative pressure (p/p₀) range 0.05-0.2, with pore size distributions determined by the
155 Barrett-Joyner-Halenda (BJH) method applied to the desorption isotherm. Thermogravimetric analysis
156 (TGA) was performed using a Mettler Toledo TGA/DSC-2 instrument under N₂ gas at 50 ml min⁻¹ and a

157 heating rate of 10 °C min⁻¹ from 25 to 900 °C. Total sulfate loadings were determined from the mass loss
158 by TGA between 600-900 °C and using a Thermo Scientific™ FLASH 2000 CHNS-O elemental analyser.
159 Metal loadings were determined using a PerkinElmer Sciex inductively coupled plasma-mass spectroscopy
160 (ICP-MS). Acid site loadings were quantified by n-propylamine chemisorption and subsequent temperature
161 programmed desorption (TPD) under flowing He at 30 ml min⁻¹ and a heating rate of 10 °C min⁻¹ from 40
162 to 800 °C. The catalyst was first saturated with n-propylamine, and physisorbed species removed by in
163 vacuo drying at 30 °C overnight [5]. Thermal desorption of reactively-formed propene (m/z=41) and
164 ammonia (m/z=17) from propylamine decomposition was monitored using a Pfeiffer ThermoStar
165 quadupole mass spectrometer.

166 **2.3 Catalyst testing**

167 **2.3.1 Esterification and transesterification of WCO**

168 WCO was obtained from a restaurant in Leeds, and contained 0.14 wt% moisture and 2 wt% FFA [5].
169 Transesterification and esterification was conducted in a stirred glass batch reactor connected to a Ministat
170 Huber 125 Pilot ONE Controller temperature controller and reflux condenser. The WCO was pre-treated
171 by simple filtration to remove physical impurities, and then heated to 100 °C to remove water.
172 Physicochemical properties of the waste cooking oil were measured after this pre-treatment. Pre-treated
173 WCO was mixed with methanol (≥99.9 %, HPLC grade Sigma-Aldrich) to achieve the desired molar ratio
174 and added to the glass reactor at room temperature, together with the desired mass of SO₄/Mg-Al-Fe₃O₄
175 catalyst. The reaction mixture was then stirred at 600 rpm and heated to the required temperature. Aliquots
176 of the mixture were periodically sampled for off-line GC-MS analysis using a Perkin Elmer Clarus 580S
177 gas chromatograph, equipped with an Elite 5ms capillary column (30.0 m x 250 μm) and a 560S mass
178 spectrometer [45].

179 **2.3.2 Esterification of oleic acid**

180 The stability of SO₄/Mg-Al-Fe₃O₄ catalyst was assessed during oleic acid esterification as a model FFA
181 using the optimised process parameters for biodiesel production from WCO. 4.0 wt% of SO₄/Mg-Al-
182 Fe₃O₄ catalyst and 9:1 molar ratio of methanol: oleic acid (Fluka Analytical, ≥99) were charged into the
183 glass reactor at room temperature. The three-phase mixture (solid-liquid-liquid) was agitated at 600 RPM
184 and heated to 95 °C. Methyl oleate formation was periodically monitored by withdrawing sample aliquots
185 and off-line GC-MS analysis [45].

186 **2.4 Biodiesel characterisation**

187 A Setaflash series 3 closed cup automated flash point tester was used to capture the flash point of the
188 synthetic biodiesel under a temperature ramp of 1-2 °C min⁻¹. The biodiesel density was calculated using a
189 pycnometric method at 15 °C, and kinematic viscosity measured at 40 °C by a Malvern Bohlin-Gemini 150
190 rotary rheometer. Acid values and %FFA of the synthetic biodiesel were measured according to standard
191 methods [5]. Free glycerol, mono-, di-, triglyceride and total glycerine contents were quantified using a
192 Perkin Elmer Clarus 560 GC equipped with an on-column injection system, a flame ionization detector and
193 a capillary column (15.0 m x 0.32 mm, 0.1 µm) [50, 51]. The total FAME (biodiesel) yield was determined
194 by off-line GC-MS using a modified EN-14103 procedure as previously reported [45] from **Equation 1**:

$$195 \text{ Total FAME \%} = \frac{(\sum A) - A_{IS}}{A_{IS}} * \frac{C_{IS} * V_{IS}}{W} * 100 \quad \text{Eqn. (1)}$$

197
198 where $\sum A$ =total peak area of methyl esters, A_{IS} =peak area of methyl heptadecanoate, C_{IS} =methyl
199 heptadecanoate concentration in mg/ml, V_{IS} =used volume of methyl heptadecanoate solution in ml, and
200 W =sample mass in mg.

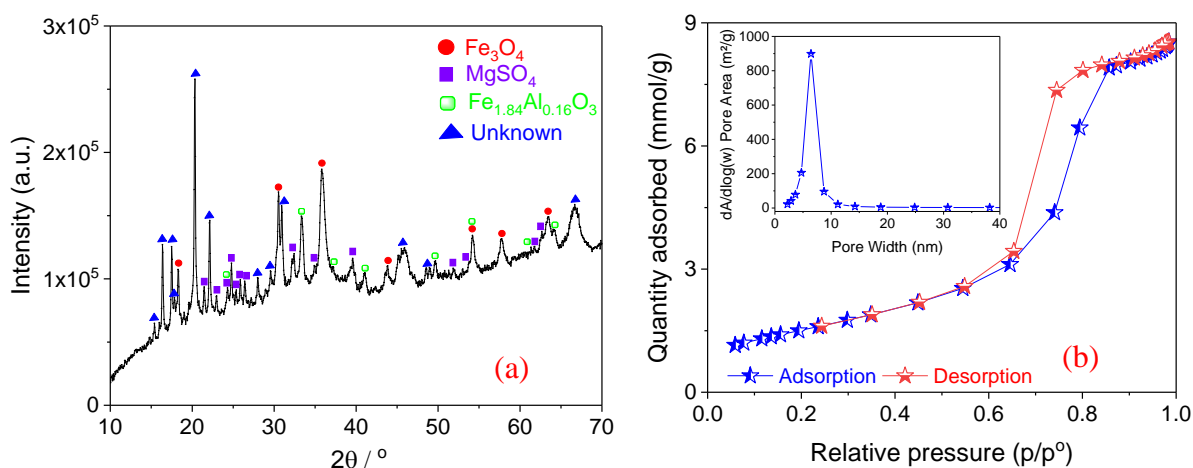
202 **2.5 Catalyst reusability and leaching**

203 Catalyst reusability for biodiesel production from WCO was assessed by magnetically separating the post-
204 reaction catalyst from the reaction mixture, washing the catalyst repeatedly with a 1:1 vol% methanol:n-
205 hexane mixture to remove any weakly bound organic residues, and then a final 250 °C re-calcination for 2
206 h to remove any chemisorbed organics, moisture or CO₂ on the catalyst surface. Leaching from the
207 SO₄/Mg-Al-Fe₃O₄ catalyst was investigated by ICP-MS. A sample of the synthetic biodiesel was digested
208 after each reaction using a HF100-multiwave 3000 (Anton Paar) microwave digester using 7.0 ml of
209 concentrated nitric acid (≥69%, Fluka Analytical, TraceSELECT®), 1.0 ml of concentrated fuming
210 hydrochloric acid (≥37%, Fluka Analytical, TraceSELECT®) and 2.0 ml of hydrogen peroxide (~30%,
211 Sigma-Aldrich, for ultra-trace analysis) reagents. The resulting solutions were diluted with deionised
212 water to 50 ml and then nebulised into the ICP. Mg, S, Al, and Fe concentrations were determined by
213 standard methods [50].

214 3. Results and discussion

215 3.1 Catalyst characterisation

216 Powder XRD of the as-prepared SO₄/Mg-Al-Fe₃O₄ (**Figure 1a**) revealed sharp reflections at 18.3, 30.2,
217 35.5, 37.2, 43.2, 53.6, 57.1, and 62.7°, assigned to the [111], [220], [311], [222], [400], [422], [511] and
218 [440] planes of cubic Fe₃O₄ (magnetite, ICDD: 04-002-3668) respectively. Particle size analysis applying
219 the Scherrer equation to peak widths indicates volume-averaged Fe₃O₄ crystalline diameters of 86 nm.
220 Reflections were also observed at 24.3, 33.4, 35.8, 41.1, 49.7, 54.4, 62.8, and 64.4° assigned to the [012],
221 [104], [110], [113], [024], [116], [214] and [300] planes respectively of rhombohedral Fe_{1.84}Al_{0.16}O₃ (iron
222 aluminium oxide, ICDD: 04-005-8669). Weak reflections are also present between 2θ=20-65°, attributed
223 to orthorhombic magnesium sulfate (MgSO₄, ICDD: 00-021-0546) with cell parameters a=4.75, b=8.59
224 and c=6.71 Å.
225



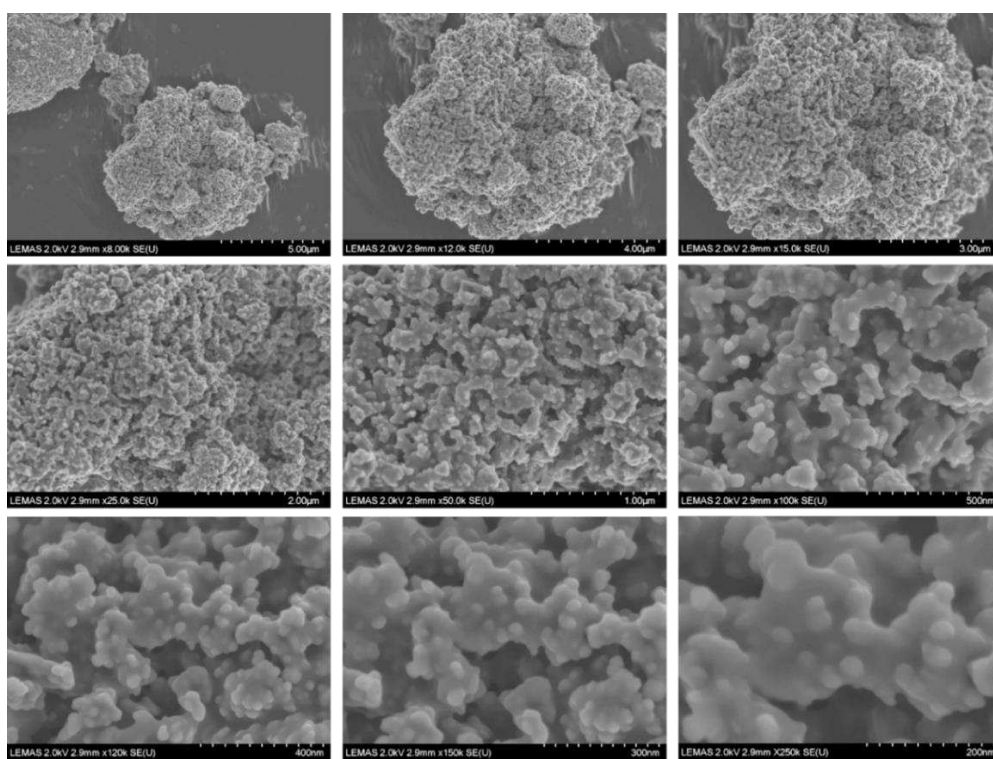
226

227 **Figure 1.** (a) Powder XRD pattern, and (b) N₂ adsorption-desorption isotherms and mean pore sizes
228 (inset) of as-prepared SO₄/Mg-Al-Fe₃O₄.

229
230

231 Porosimetry of SO₄/Mg-Al-Fe₃O₄ showed a Type IV isotherm (**Figure 1b**) and type H1 hysteresis loop
232 [52] which are typically associated with capillary condensation within cylindrical mesopores. Since the
233 synthesis did not employ a structure-directing template, these mesopores may arise from interparticle voids,
234 but in any even could serve to improve reactant accessibility to active sites. SEM images of the SO₄/Mg-
235 Al-Fe₃O₄ catalyst reveal the formation of large (~20-40 nm) nanoparticle aggregates (**Figure 2**) which are
236 embedded in a (presumably amorphous alumina and/or MgSO₄) matrix to form a coral-like porous
237 architecture. TEM images confirm the presence of (high contrast) Fe₃O₄ cores between 20-150 nm

238 diameter, encapsulated by amorphous shells comprising low contrast aggregates of (presumably Al/Mg-
239 rich) of ~5-15 nm nanoparticles (**Figure 3**). Elemental maps confirm that Fe₃O₄ nanoparticles are
240 embedded within an Al-rich matrix (**Figure 4**), with Mg co-located with S in a 1:1 atomic ratio. The
241 atomic ratio of Al:Mg = 6:1 throughout the sample which may suppress nucleation and growth of Mg-Al
242 hydrotalcites (unstable for values >4:1), whereas that for Fe:Mg = 3:1 [53]. The low magnesium content
243 of the as-prepared catalyst may also reflect the low pH used during its synthesis. The total sulfur content
244 determined by TEM-EDS, CHNS-O, and ICP-MS was approximately 7 wt% (**Table 1**), higher than that
245 reported for SO₄/MO_x (2-3 wt%) [54] and Al-doped SO₄/ZrO₂ (1.5 wt%) [55], but comparable to SO₄/Fe-
246 Al-TiO₂ [5].



247

248

249

250

Figure 2. SEM images at different magnifications for SO₄/Mg-Al-Fe₃O₄ catalyst.

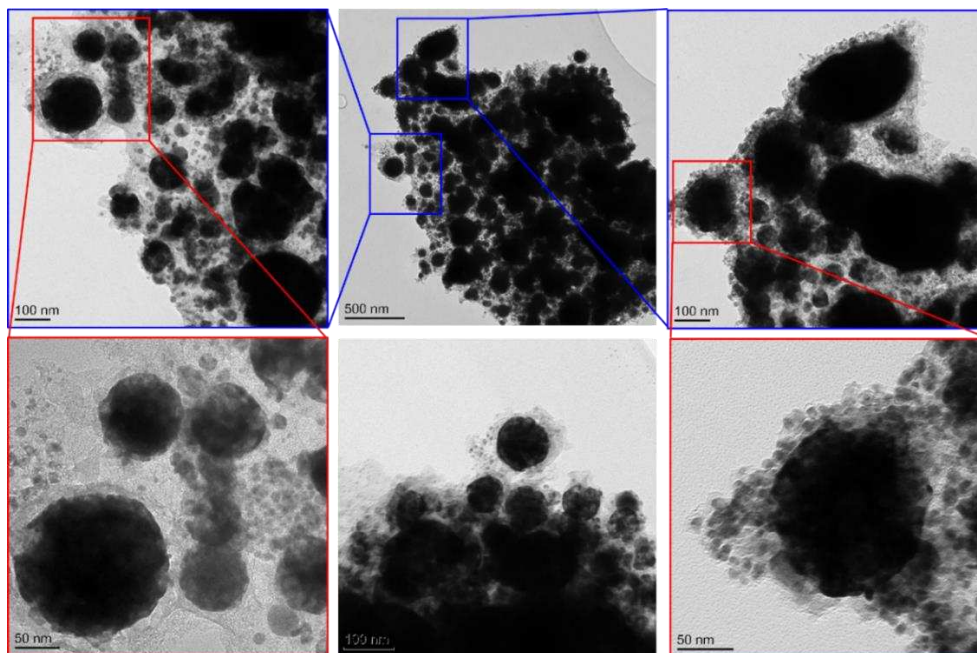


Figure 3. TEM images of $\text{SO}_4/\text{Mg-Al-Fe}_3\text{O}_4$ catalyst.

Table 1. Textural properties and composition of $\text{SO}_4/\text{Mg-Al-Fe}_3\text{O}_4$.

	Textural properties ^a			Composition / atom% ^b					Bulk S content/ wt%	
	$S_{\text{BET}} / \text{m}^2 \text{g}^{-1}$	D_p / nm	$V_p / \text{cm}^3 \text{g}^{-1}$	O	Mg	Al	S	Fe		
$\text{SO}_4/\text{Mg-Al-Fe}_3\text{O}_4$	123 ± 1	6.5 ± 0.5	0.3	60.5	3.5	20.7	4.6	10.7	7.8 ± 1^c	7.6 ± 0.5^d

^a N_2 porosimetry. ^bEDS. ^cCHNS-O. ^dICP-MS.

The ATR-IR spectrum of $\text{SO}_4/\text{Mg-Al-Fe}_3\text{O}_4$ exhibited a strong broad band at 3252 cm^{-1} attributed to the O-H stretch of physisorbed water (**Figure 5a**) on the surface of the catalyst from the air and/or interlayer water molecules while the peak at 3072 cm^{-1} corresponded to the O-H stretching vibration of bound water [5, 38, 56]. The strong bands between $982\text{-}1087 \text{ cm}^{-1}$ are assigned to chelating bidentate sulfate (SO_4^{2-}) and/or chelating double-bridge peroxydisulfate ($\text{S}_2\text{O}_8^{2-}$) groups, and that at 1418 cm^{-1} to an S=O stretch [38, 39]. Bands at $719, 604,$ and 566 cm^{-1} likely arise from to M-O-M stretches involving Al-O, Mg-O and Fe-O bonds [38, 56-59].

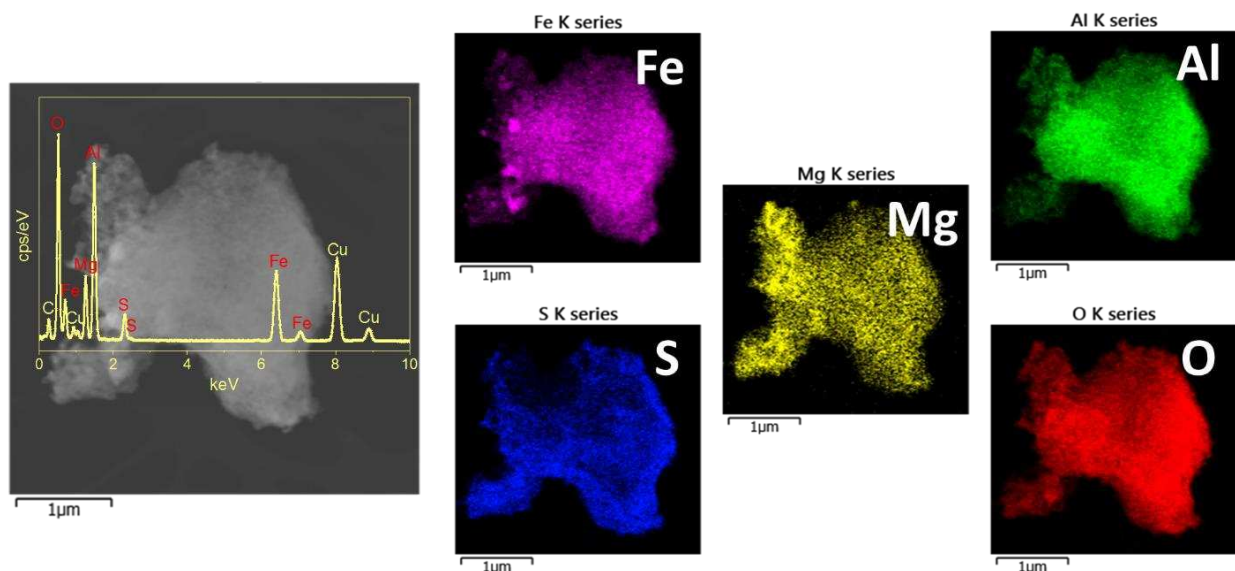


Figure 4. EDS elemental mapping of $\text{SO}_4/\text{Mg-Al-Fe}_3\text{O}_4$ catalyst.

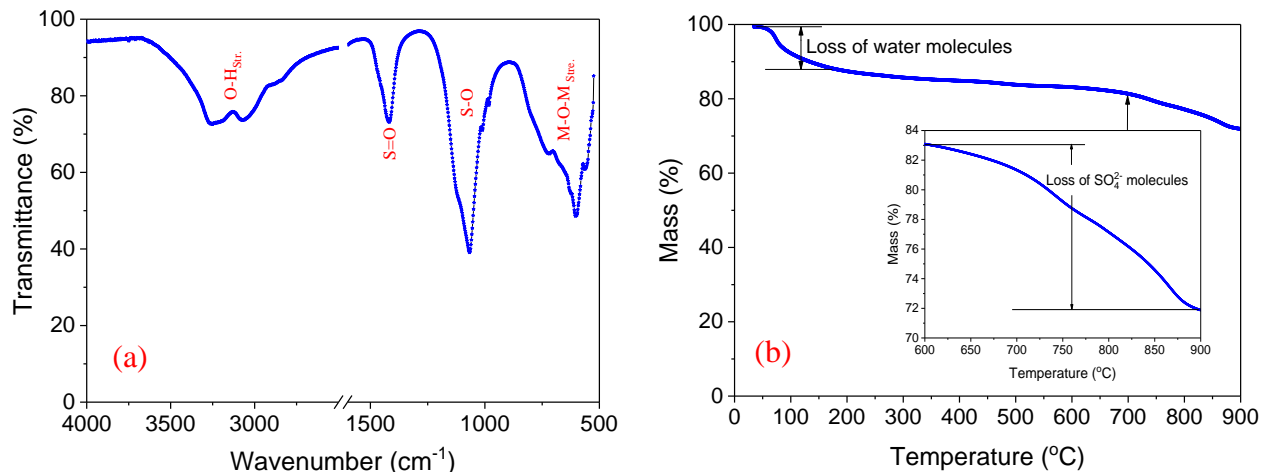
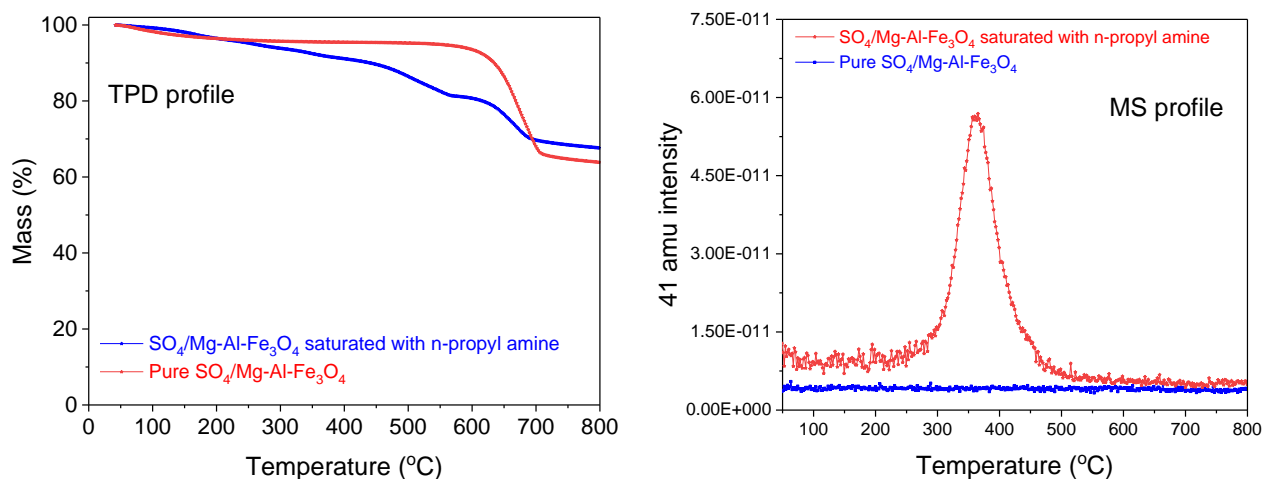


Figure 5. (a) FTIR spectrum and (b) TGA profile of $\text{SO}_4/\text{Mg-Al-Fe}_3\text{O}_4$.

TGA of the as-prepared $\text{SO}_4/\text{Mg-Al-Fe}_3\text{O}_4$ exhibited two distinct weight losses (**Figure 5b**). The first, between 100 and 150 °C, is associated with the loss of physisorbed water [60], and the second between 600-900 °C is due to the decomposition of sulfate and/or peroxydisulfate groups and SO_x evolution [5]; sulfate species are thermally stable <600 °C, superior to that observed for other sulfated metal oxides [39, 61]. The sulfate loading calculated from TGA of 11 wt% is in good agreement with elemental analysis. Acid loading and strength of the as-prepared catalyst were quantified by n-propylamine TPD-MS (**Figure 6**). A strong desorption peak for reactively-formed propene is observed between 300-500 °C (arising from

279 Hofmann elimination of chemisorbed n-propylamine over acid sites) indicative of moderate strength acid
280 sites akin to those reported in SO_4/ZrO_2 [32]. The calculated total acidic site loadings of the $\text{SO}_4/\text{Mg-Al-Fe}_3\text{O}_4$
281 Fe_3O_4 catalyst were found to be 2.35 mmol g^{-1} which is much higher than that reported for other sulfated
282 metal oxides (typically $<1 \text{ mmol g}^{-1}$) [5, 62, 63].
283



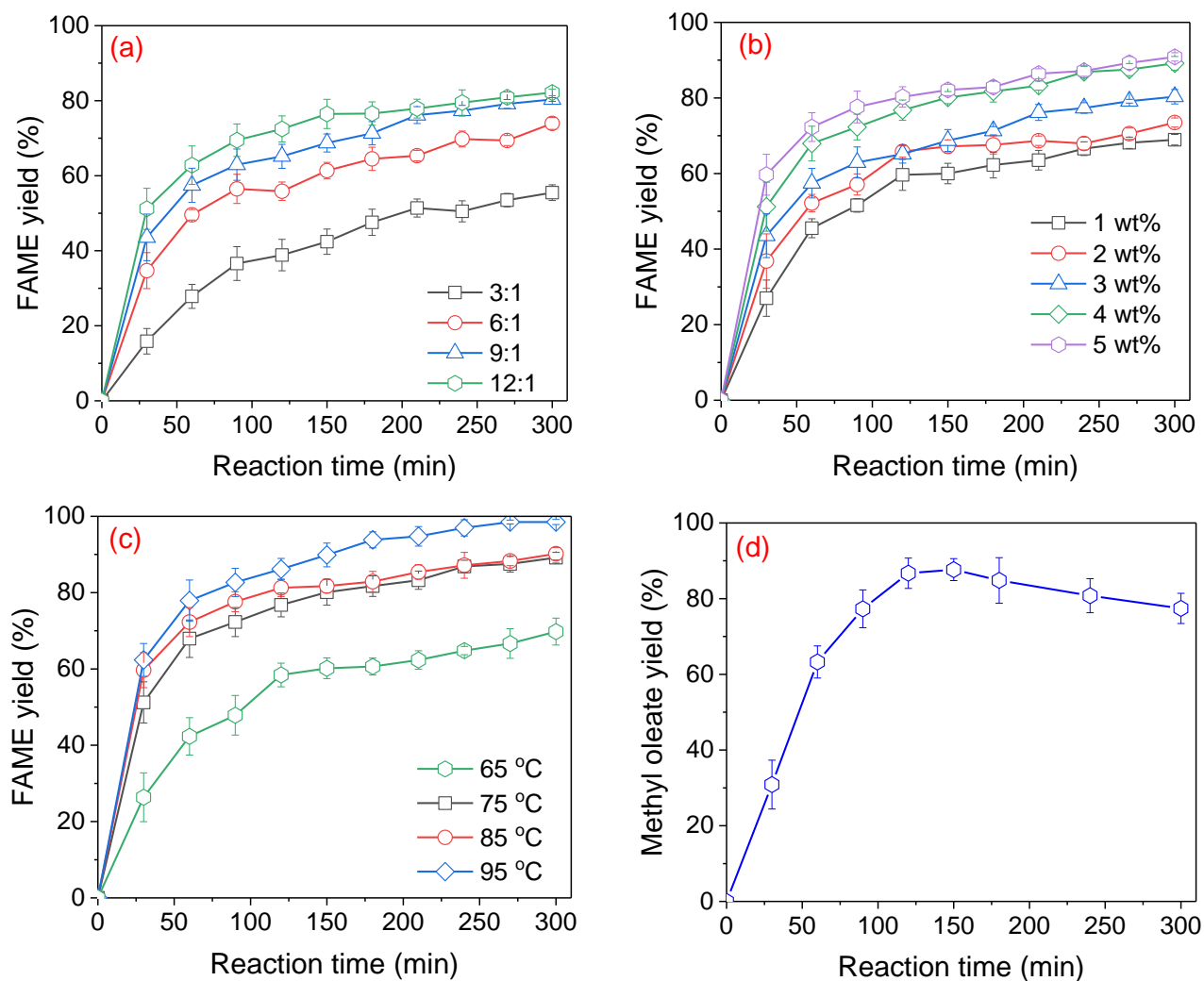
284
285 **Figure 6.** (left) TPD profiles, and (right) mass spectra for $\text{SO}_4/\text{Mg-Al-Fe}_3\text{O}_4$ catalyst of pure and
286 saturated with n-propylamine.
287

287

288 3.2 Catalytic performance

289 The as-prepared $\text{SO}_4/\text{Mg-Al-Fe}_3\text{O}_4$ catalyst was subsequently evaluated for biodiesel production from
290 WCO (**Figure 7**). First, the effect of methanol:WCO molar ratio was explored between 3:1 to 12:1;
291 increasing the methanol content monotonically enhanced the 6 h FAME yield from approximately 55 to
292 80 % by shifting the transesterification reaction equilibrium (**Figure 7a**). Since only a small yield
293 enhancement was observed for methanol:WCO ratios $>9:1$, this reaction composition was employed for
294 all further experiments. Increasing the catalyst mass (with respect to WCO) from 1 to 5 wt% linearly
295 improved the initial FAME yield (**Figure 7b**), indicating that transesterification was free from mass-
296 transport limitations during the first hour of reaction reflecting the rise in active sites preceding a slow
297 deactivation at longer reaction times [64]. Final 6 h FAME yields spanned 65-80 %. A catalyst loading of
298 3 wt% was selected as this provided a sufficient yield to measure accurately, while offering scope for
299 improvements during further optimisation without encountering diffusion limitations. The impact of
300 reaction temperatures was also studied between 65 to 95 °C (**Figure 7c**) [45]. A significant yield increase
301 was observed on raising the reaction temperature to 75 °C (followed by a more gradual rise at higher

302 temperature) which may both reflect both enhanced rates of TAG hydrolysis and better miscibility of the
 303 methanol/WCO liquid phases, as previously reported [65, 66]. The maximum 6 h FAME yield >95 % at
 304 the highest temperature. To establish the catalyst tolerance to FFAs, oleic acid esterification with methanol
 305 was also examined under the optimum reaction conditions (**Figure 7d**). $\text{SO}_4/\text{Mg-Al-Fe}_3\text{O}_4$ catalyst was
 306 active for methyl oleate production, with a maximum FAME yield of 87 % after 2 h reaction; the small
 307 drop in FAME yield at longer reaction times may be associated with water (by-product) accumulation
 308 driving the reverse hydrolysis.

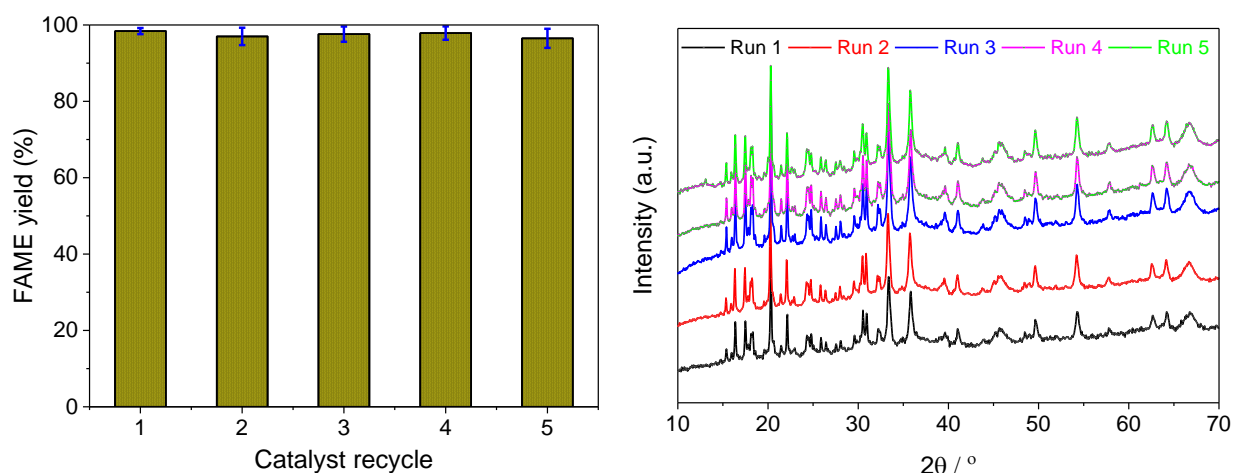


310
 311 **Figure 7.** WCO transesterification over $\text{SO}_4/\text{Mg-Al-Fe}_3\text{O}_4$ as a function of (a) methanol:WCO molar
 312 ratio at 75 °C and 3 wt% catalyst, (b) catalyst loading at 75 °C and 9:1 methanol:WCO molar ratio, and
 313 (c) reaction temperature at 4 wt% catalyst and 9:1 methanol:WCO molar ratio. (d) Oleic acid
 314 esterification over $\text{SO}_4/\text{Mg-Al-Fe}_3\text{O}_4$ at 95 °C, 4 wt% catalyst, and 9:1 methanol:oleic acid molar ratio.

315

316 3.3 Magnetic catalyst reusability and leaching

317 Stability of $\text{SO}_4/\text{Mg-Al-Fe}_3\text{O}_4$ for WCO transesterification was investigated during five catalyst re-uses
 318 under optimal reaction conditions (**Figure 8**). Minimal deactivation was observed, consistent with post-
 319 reaction XRD analysis of the catalyst which evidenced negligible change in the phase or crystallinity, and
 320 elemental analysis which revealed negligible metal or sulfur leaching occurred into the reaction medium
 321 (**Table 2**). A small increase in the residual Al and Fe concentrations in the biodiesel product was observed
 322 for Run 3, attributed to the use of a different strength magnet to separate the nanoparticles compared with
 323 the other four runs. This excellent stability is an important consideration for commercial (large scale)
 324 biodiesel production from low grade oil feedstocks.



326
 327 **Figure 8. (left)** Transesterification of WCO over $\text{SO}_4/\text{Mg-Al-Fe}_3\text{O}_4$ as a function of re-use: reaction
 328 conditions: 4 wt%, 95 °C, 9:1 methanol:WCO molar ratio. **(right)** XRD patterns of post-reaction
 329 $\text{SO}_4/\text{Mg-Al-Fe}_3\text{O}_4$.

330
 331
 332 **Table 2.** Elemental analysis of biodiesel after magnetic catalyst separation.

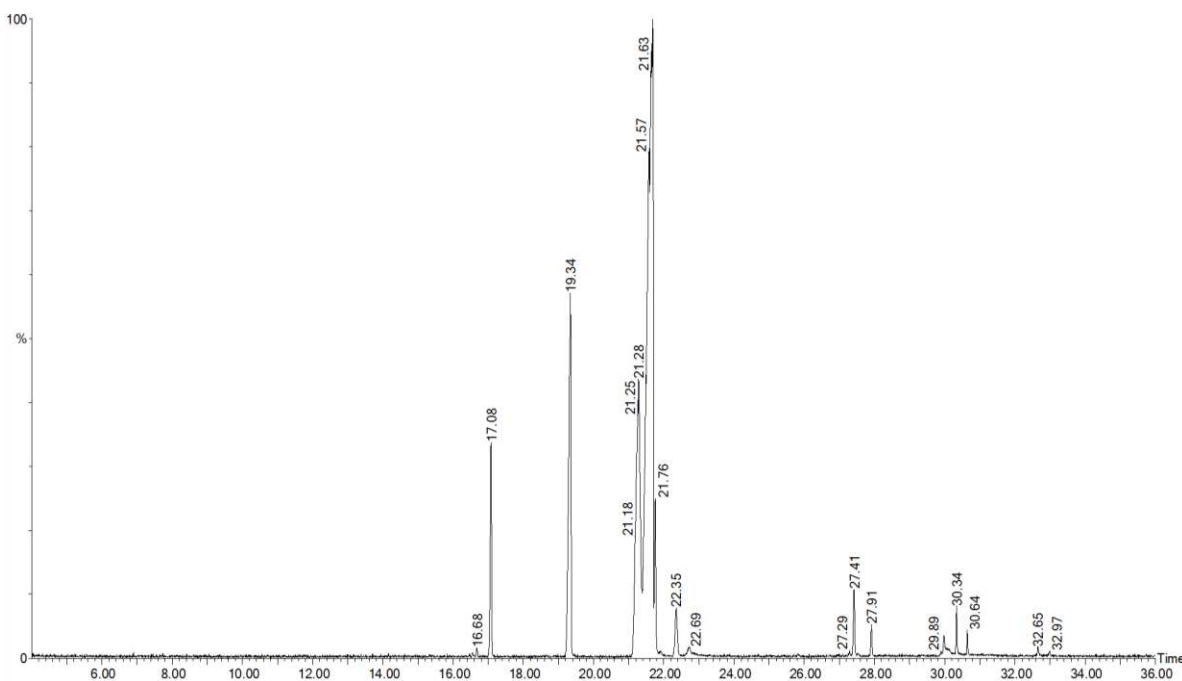
		Leachate concentration ^a / $\mu\text{g L}^{-1}$			
		Mg	Al	S	Fe
Spent catalyst	Run 1	0.343	0.124	0.000	0.082
	Run 2	0.308	0.098	0.000	0.028
	Run 3	0.356	0.378	0.000	0.229
	Run 4	0.327	0.120	0.000	0.067
	Run 5	0.220	0.082	0.000	0.053

333 ^a ICP-MS.

334 **3.3 Biodiesel characterisation**

335 Analysis of the transesterification biodiesel product is critical to determining the quality of any ultimate
336 fuel blend due to the potential presence of contaminants including glycerol, FFAs, catalyst residue,
337 methanol, and water. GC-MS analysis (**Figure 9**) of the biodiesel product was therefore conducted to
338 quantify the biodiesel purity, using a response factor from the methyl heptanoate internal standard (≥ 99.5
339 purity, Sigma-Aldrich) to calculate the amount of individual FAME components (**Table 3**). The major
340 FAME products were methyl palmitate, methyl stearate, methyl oleate, methyl linoleate, methyl linoleate,
341 and methyl gadoleate. The physicochemical properties of the biodiesel confirm that its quality meets
342 ASTM and EU standards (**Table 4**).

343



344

345 **Figure 9.** GC-MS chromatogram for biodiesel product from WCO transesterification over $\text{SO}_4/\text{Mg-Al-Fe}_3\text{O}_4$. Reaction conditions: 4 wt% catalyst mass to WCO, 95 °C, 9:1 methanol:WCO molar ratio

346

347

348

349

350

351

352

353

Table 3. FAME composition of biodiesel derived from WCO transesterification over $\text{SO}_4/\text{Mg-Al-Fe}_3\text{O}_4$

FAME	Chain structure	Retention time / mins	Area	FAME / Area %
Myristic acid methyl ester	C _{14:0}	14.157	528458	0.04
Palmitic acid methyl ester	C _{16:0}	17.074	66629604	5.01
Palmitoleic acid methyl ester	C _{16:1}	16.673	2244707	0.17
Heptadecanoic acid methyl ester	C _{17:0}	19.334	195359776	IS
Stearic acid methyl ester	C _{18:0}	22.351	26016648	1.96
Oleic acid methyl ester	C _{18:1}	21.675	898642007	67.77
Linoleic acid methyl ester	C _{18:2}	21.280	279073632	20.99
Linolenic acid methyl ester	C _{18:3}	21.675	17771433	1.17
Gadoleic acid methyl ester	C _{20:1}	27.413	20598874	1.55
Erucic acid methyl ester	C _{21:1}	30.334	11479104	0.86
Behenic acid methyl ester	C _{22:0}	30.639	5037719	0.38
Lignoceric acid methyl ester	C _{24:0}	30.980	1328256	0.10

354

355

356

Table 4. Properties of biodiesel derived from WCO transesterification over $\text{SO}_4/\text{Mg-Al-Fe}_3\text{O}_4$

Property	Unit	Limits		Synthesised biodiesel
		ASTM D6751	EN14214	
Flash point	°C	93 min.	101 min.	179.5
Kinematic viscosity	mm ² s ⁻¹	1.9-6.0	3.5-5.0	4.74
Acid number	mgKOH g ⁻¹	0.8 max.	0.5 max.	0.34
Density at 15 °C	kg m ⁻³	---	860-900	892.6
FAME content	% mass	---	96.5 min.	98.5
Methyl linolenate content	% mass	---	12 max.	1.17
Free glycerine content	% mass	0.02 max.	---	0.025
Total glycerine content	% mass	0.24 max.	0.25 max.	0.122
Monoglyceride content	% mass	---	0.8 max.	0.007
Diglyceride content	% mass	---	0.2 max.	0.008
Triglyceride content	% mass	---	0.2 max.	0.082

357

4. Conclusions

358

359

360

361

A novel magnetically separable $\text{SO}_4/\text{Mg-Al-Fe}_3\text{O}_4$ core-shell catalyst was synthesised for the transesterification of WCO and esterification of oleic acid. Bulks and surface physicochemical properties were characterised by XRD, SEM, TEM, TGA, ATR-FTIR, N_2 porosimetry, and propylamine TPD-MS. Magnetic Fe_3O_4 (20-150 nm diameter) nanoparticles were encapsulated by 5-15 nm thick alumina and/or

362 MgSO₄ shells. Sulfation generated surface bidentate sulfate ions which exhibited moderate acid strengths
363 but high acid site loadings of 2.35 mmol g⁻¹. The multifunctional catalyst properties (super acidity and
364 magnetic separability) pave the way for simultaneous esterification and transesterification of low grade
365 bio-oil feedstocks to biodiesel, eliminating the need for current pre-treatments to reduce the FFA content,
366 and enabling facile and energy efficient product separation. The SO₄/Mg-Al-Fe₃O₄ catalyst exhibited good
367 activity for biodiesel production from WCO for a 9:1 methanol:oil molar ratio and 4 wt% catalyst loading
368 after 5 h reaction at 95 °C. It also exhibited good activity for oleic acid esterification (87 % yield in 2 h)
369 under similar reaction conditions, highlighting the potential of SO₄/Mg-Al-Fe₃O₄ for the direct conversion
370 of low grade oil feedstocks high in FFAs to biodiesel, without requiring any pre-treatment. SO₄/Mg-Al-
371 Fe₃O₄ demonstrates excellent stability and recyclability over five consecutive transesterification reactions
372 with negligible deactivation or leaching, paving the way to commercial biodiesel production from WCO
373 using a heterogeneous catalyst. Future study could involve investigation of the effect of different
374 calcination temperatures on the catalytic performance of this magnetic catalyst. An extended study should
375 also focus on the investigation of mechanism of this catalyst for esterification and transesterification
376 reactions. Tests of different chain length of fatty acid composition feedstocks need to be carried out in
377 order to better understand its effect on the performance of this type of catalyst as WCO is a mixture of
378 different fatty acids.

379

380 **Acknowledgments**

381 The authors are gratefully acknowledge the Ministry of Higher Education and Scientific Research of the
382 Kurdistan Regional Government for funding this study under the Human Capacity Development Program
383 (HCDP).

384

385 **Conflicts of interest**

386 The authors declare no conflict of interest.

387

388 References

- 389 1. Atabani, A.E., A.S. Silitonga, I.A. Badruddin, T. Mahlia, H. Masjuki, and S. Mekhilef, A
390 comprehensive review on biodiesel as an alternative energy resource and its characteristics.
391 Renewable and sustainable energy reviews, **2012**. 16(4): p. 2070-2093.
- 392 2. Wilson, K. and A.F. Lee, Rational design of heterogeneous catalysts for biodiesel synthesis.
393 Catalysis Science & Technology, **2012**. 2(5): p. 884-897.
- 394 3. Melero, J.A., L.F. Bautista, G. Morales, J. Iglesias, and R. Sánchez-Vázquez, Biodiesel production
395 from crude palm oil using sulfonic acid-modified mesostructured catalysts. Chemical Engineering
396 Journal, **2010**. 161(3): p. 323-331.
- 397 4. Younis, K.A., J.L. Gardy, and K.S. Barzinji, Production and characterization of biodiesel from
398 locally sourced sesame seed oil, used cooking oil and other commercial vegetable oils in Erbil-
399 Iraqi Kurdistan. American Journal of Applied Chemistry, **2014**. 2(6): p. 105-111.
- 400 5. Gardy, J., A. Osatiashtiani, O. Céspedes, A. Hassanpour, X. Lai, A.F. Lee, K. Wilson, and M.
401 Rehan, A magnetically separable $SO_4/Fe-Al-TiO_2$ solid acid catalyst for biodiesel production from
402 waste cooking oil. Applied Catalysis B: Environmental, **2018**. 234: p. 268-278.
- 403 6. Gardy, J., A. Hassanpour, X. Lai, and M. Rehan, The influence of blending process on the quality
404 of rapeseed oil-used cooking oil biodiesels. International Scientific Journal (Journal of
405 Environmental Science), **2014**. 3: p. 233-240.
- 406 7. Silva, Â., K. Wilson, A.F. Lee, V.C. dos Santos, A.C.C. Bacilla, K.M. Mantovani, and S.
407 Nakagaki, $Nb_2O_5/SBA-15$ catalyzed propanoic acid esterification. Applied Catalysis B:
408 Environmental, **2017**. 205: p. 498-504.
- 409 8. Creasey, J.J., A. Chiericato, J.C. Manayil, C.M. Parlett, K. Wilson, and A.F. Lee, Alkali-and
410 nitrate-free synthesis of highly active Mg–Al hydrotalcite-coated alumina for FAME production.
411 Catalysis Science & Technology, **2014**. 4(3): p. 861-870.
- 412 9. Rehan, M., J. Gardy, A. Demirbas, U. Rashid, W. Budzianowski, D. Pant, and A. Nizami, Waste
413 to biodiesel: A preliminary assessment for Saudi Arabia. Bioresource technology, **2018**. 250: p.
414 17-25.
- 415 10. Alhassan, F.H., U. Rashid, and Y.H. Taufiq-Yap, Synthesis of waste cooking oil based biodiesel
416 via ferric-manganese promoted molybdenum oxide/zirconia nanoparticle solid acid catalyst:
417 influence of ferric and manganese dopants. Journal of oleo science, **2015**. 64(5): p. 505-514.
- 418 11. Nisar, J., R. Razaq, M. Farooq, M. Iqbal, R.A. Khan, M. Sayed, A. Shah, and I. ur Rahman,
419 Enhanced biodiesel production from Jatropha oil using calcined waste animal bones as catalyst.
420 Renewable Energy, **2017**. 101: p. 111-119.
- 421 12. Li, L., C. Zou, L. Zhou, and L. Lin, Cucurbituril-protected $Cs_{2.5}H_{0.5}PW_{12}O_{40}$ for optimized
422 biodiesel production from waste cooking oil. Renewable energy, **2017**. 107: p. 14-22.
- 423 13. Lee, A.F., Catalysing sustainable fuel and chemical synthesis. Applied Petrochemical Research,
424 **2014**. 4(1): p. 11-31.
- 425 14. Raia, R.Z., L.S. da Silva, S.M.P. Marcucci, and P.A. Arroyo, Biodiesel production from Jatropha
426 curcas L. oil by simultaneous esterification and transesterification using sulphated zirconia.
427 Catalysis Today, **2017**. 289: p. 105-114.
- 428 15. Upham, P., P. Thornley, J. Tomei, and P. Boucher, Substitutable biodiesel feedstocks for the UK:
429 a review of sustainability issues with reference to the UK RTFO. Journal of Cleaner Production,
430 **2009**. 17: p. S37-S45.

- 431 16. Pirez, C., A. Lee, J.C. Manayil, C. Parlett, and K. Wilson, Hydrothermal saline promoted grafting:
432 a route to sulfonic acid SBA-15 silica with ultra-high acid site loading for biodiesel synthesis.
433 *Green Chemistry*, **2014**. 16(10): p. 4506-4509.
- 434 17. Montero, J., M. Isaacs, A. Lee, J. Lynam, and K. Wilson, The surface chemistry of nanocrystalline
435 MgO catalysts for FAME production: An in situ XPS study of H₂O, CH₃OH and CH₃OAc
436 adsorption. *Surface Science*, **2016**. 646: p. 170-178.
- 437 18. Lee, A.F. and K. Wilson, Recent developments in heterogeneous catalysis for the sustainable
438 production of biodiesel. *Catalysis Today*, **2015**. 242: p. 3-18.
- 439 19. Komintarachat, C. and S. Chuepeng, Solid acid catalyst for biodiesel production from waste used
440 cooking oils. *Industrial & Engineering Chemistry Research*, **2009**. 48(20): p. 9350-9353.
- 441 20. Eze, V.C., A.N. Phan, C. Pirez, A.P. Harvey, A.F. Lee, and K. Wilson, Heterogeneous catalysis
442 in an oscillatory baffled flow reactor. *Catalysis Science & Technology*, **2013**. 3(9): p. 2373-2379.
- 443 21. Lee, A.F., J.A. Bennett, J.C. Manayil, and K. Wilson, Heterogeneous catalysis for sustainable
444 biodiesel production via esterification and transesterification. *Chemical Society Reviews*, **2014**.
445 43(22): p. 7887-7916.
- 446 22. Sharma, Y.C., B. Singh, and J. Korstad, Advancements in solid acid catalysts for ecofriendly and
447 economically viable synthesis of biodiesel. *Biofuels, Bioproducts and Biorefining*, **2011**. 5(1): p.
448 69-92.
- 449 23. Gardy, J., A. Hassanpour, X. Lai, M.H. Ahmed, and M. Rehan, Biodiesel production from used
450 cooking oil using a novel surface functionalised TiO₂ nano-catalyst. *Applied Catalysis B:
451 Environmental*, **2017**. 207: p. 297-310.
- 452 24. Sani, Y.M., W.M.A.W. Daud, and A.A. Aziz, Activity of solid acid catalysts for biodiesel
453 production: a critical review. *Applied Catalysis A: General*, **2014**. 470: p. 140-161.
- 454 25. Melero, J.A., J. Iglesias, and G. Morales, Heterogeneous acid catalysts for biodiesel production:
455 Current status and future challenges. *Green Chemistry*, **2009**. 11(9): p. 1285-1308.
- 456 26. Farabi, M.A., M.L. Ibrahim, U. Rashid, and Y.H. Taufiq-Yap, Esterification of palm fatty acid
457 distillate using sulfonated carbon-based catalyst derived from palm kernel shell and bamboo.
458 *Energy Conversion and Management*, **2019**. 181: p. 562-570.
- 459 27. Zhang, J., A. Motta, Y. Gao, M.M. Stalzer, M. Delferro, B. Liu, T.L. Lohr, and T.J. Marks,
460 Cationic pyridylamido adsorbate on Brønsted acidic sulfated zirconia: A molecular supported
461 organohafnium catalyst for olefin homo- and co-polymerization. *ACS Catalysis*, **2018**.
- 462 28. Arfaoui, J., A. Ghorbel, C. Petitto, and G. Delahay, Novel V₂O₅-CeO₂-TiO₂-SO₄²⁻ nanostructured
463 aerogel catalyst for the low temperature selective catalytic reduction of NO by NH₃ in excess O₂.
464 *Applied Catalysis B: Environmental*, **2018**. 224: p. 264-275.
- 465 29. Xu, D., X. Lai, W. Guo, X. Zhang, C. Wang, and P. Dai, Efficient catalytic properties of
466 SO₄²⁻/MxOy (M= Cu, Co, Fe) catalysts for hydrogen generation by methanolysis of sodium
467 borohydride. *International Journal of Hydrogen Energy*, **2018**. 43(13): p. 6594-6602.
- 468 30. Kaur, K., A. Sobti, R.K. Wanchoo, and A.P. Toor, Studies on glycerol conversion to tricaproin
469 over sulfate promoted iron oxide as catalyst using response surface methodology. *Chemical
470 Engineering Research and Design*, **2018**.
- 471 31. Li, S., H. Song, Y. Hu, F. Li, and Y. Chen, A novel method for the synthesis of highly stable nickel-
472 modified sulfated zirconia catalysts for n-pentane isomerization. *Catalysis Communications*, **2018**.
473 104: p. 57-61.
- 474 32. Osatiashtiani, A., L.J. Durndell, J.C. Manayil, A.F. Lee, and K. Wilson, Influence of alkyl chain
475 length on sulfated zirconia catalysed batch and continuous esterification of carboxylic acids by
476 light alcohols. *Green Chemistry*, **2016**. 18(20): p. 5529-5535.

- 477 33. de Almeida, R.M., L.K. Noda, N.S. Goncalves, S.M. Meneghetti, and M.R. Meneghetti,
478 Transesterification reaction of vegetable oils, using superacid sulfated TiO₂-base catalysts.
479 Applied Catalysis A: General, **2008**. 347(1): p. 100-105.
- 480 34. Rabee, A.I., G.A. Mekhemer, A. Osatiashtiani, M.A. Isaacs, A.F. Lee, K. Wilson, and M.I. Zaki,
481 Acidity-reactivity relationships in catalytic esterification over ammonium sulfate-derived sulfated
482 zirconia. Catalysts, **2017**. 7(7): p. 204.
- 483 35. Noda, L.K., R.M. de Almeida, N.S. Gonçalves, L.F.D. Probst, and O. Sala, TiO₂ with a high sulfate
484 content—thermogravimetric analysis, determination of acid sites by infrared spectroscopy and
485 catalytic activity. Catalysis today, **2003**. 85(1): p. 69-74.
- 486 36. Osatiashtiani, A., A.F. Lee, D.R. Brown, J.A. Melero, G. Morales, and K. Wilson, Bifunctional
487 SO₄/ZrO₂ catalysts for 5-hydroxymethylfurfural (5-HMF) production from glucose. Catalysis
488 Science & Technology, **2014**. 4(2): p. 333-342.
- 489 37. Alhassan, F.H., U. Rashid, and Y. Taufiq-Yap, Synthesis of waste cooking oil-based biodiesel via
490 effectual recyclable bi-functional Fe₂O₃-MnO-SO₄²⁻/ZrO₂ nanoparticle solid catalyst. Fuel, **2015**.
491 142: p. 38-45.
- 492 38. Wu, H., Y. Liu, J. Zhang, and G. Li, In situ reactive extraction of cottonseeds with methyl acetate
493 for biodiesel production using magnetic solid acid catalysts. Bioresource technology, **2014**. 174:
494 p. 182-189.
- 495 39. Guan, D., M. Fan, J. Wang, Y. Zhang, Q. Liu, and X. Jing, Synthesis and properties of magnetic
496 solid superacid: SO₄²⁻/ZrO₂-B₂O₃-Fe₃O₄. Materials Chemistry and Physics, **2010**. 122(1): p. 278-
497 283.
- 498 40. Li, J. and X. Liang, Magnetic solid acid catalyst for biodiesel synthesis from waste oil. Energy
499 Conversion and Management, **2017**. 141: p. 126-132.
- 500 41. Zillillah, G. Tan, and Z. Li, Highly active, stable, and recyclable magnetic nano-size solid acid
501 catalysts: efficient esterification of free fatty acid in grease to produce biodiesel. Green Chemistry,
502 **2012**. 14(11): p. 3077-3086.
- 503 42. Liu, W.-J., K. Tian, H. Jiang, and H.-Q. Yu, Facile synthesis of highly efficient and recyclable
504 magnetic solid acid from biomass waste. Scientific Reports, **2013**. 3: p. 2419.
- 505 43. Wang, Y.-T., X.-X. Yang, J. Xu, H.-L. Wang, Z.-B. Wang, L. Zhang, S.-L. Wang, and J.-L. Liang,
506 Biodiesel production from esterification of oleic acid by a sulfonated magnetic solid acid catalyst.
507 Renewable Energy, **2019**. 139: p. 688-695.
- 508 44. Lai, D.-m., L. Deng, Q.-x. Guo, and Y. Fu, Hydrolysis of biomass by magnetic solid acid. Energy
509 & Environmental Science, **2011**. 4(9): p. 3552-3557.
- 510 45. Gardy, J., A. Hassanpour, X. Lai, and M.H. Ahmed, Synthesis of Ti(SO₄)O solid acid nano-catalyst
511 and its application for biodiesel production from used cooking oil. Applied Catalysis A: General,
512 **2016**. 527: p. 81-95.
- 513 46. Roper-Vega, J., A. Aldana-Pérez, R. Gómez, and M. Niño-Gómez, Sulfated titania [TiO₂/SO₄²⁻]:
514 a very active solid acid catalyst for the esterification of free fatty acids with ethanol. Applied
515 Catalysis A: General, **2010**. 379(1-2): p. 24-29.
- 516 47. Shao, G.N., R. Sheikh, A. Hilonga, J.E. Lee, Y.-H. Park, and H.T. Kim, Biodiesel production by
517 sulfated mesoporous titania-silica catalysts synthesized by the sol-gel process from less expensive
518 precursors. Chemical engineering journal, **2013**. 215: p. 600-607.
- 519 48. Tai, Z., M.A. Isaacs, C.M. Parlett, A.F. Lee, and K. Wilson, High activity magnetic core-
520 mesoporous shell sulfonic acid silica nanoparticles for carboxylic acid esterification. Catalysis
521 Communications, **2017**. 92: p. 56-60.

- 522 49. Saravanan, K., B. Tyagi, R.S. Shukla, and H. Bajaj, Esterification of palmitic acid with methanol
523 over template-assisted mesoporous sulfated zirconia solid acid catalyst. *Applied Catalysis B:*
524 *Environmental*, **2015**. 172: p. 108-115.
- 525 50. Gardy, J.L.I.A., Biodiesel production from used cooking oil using novel solid acid catalysts, in
526 Faculty of Engineering; School of Chemical and Process Engineering **2017**, The University of
527 Leeds Whiterose e-theses, Leeds, UK.
- 528 51. EN-14105, Fat and oil derivatives. Fatty acid methyl esters (FAME). Determination of free and
529 total glycerol and mono-, di-, triglyceride contents. **2011**. p. 1-26.
- 530 52. Klobes, P., K. Meyer, and R.G. Munro, Porosity and specific surface area measurements for solid
531 materials. **2006**, National Institute of Standards and Technology: U.S. p. 89.
- 532 53. Yuan, C., H. Liu, and X. Gao, Magnetically recoverable heterogeneous catalyst: Tungstate
533 intercalated Mg–Al-layered double hydroxides-encapsulated Fe₃O₄ nanoparticles for highly
534 efficient selective oxidation of sulfides with H₂O₂. *Catalysis letters*, **2014**. 144(1): p. 16-21.
- 535 54. Kiss, A.A., F. Omota, A.C. Dimian, and G. Rothenberg, The heterogeneous advantage: biodiesel
536 by catalytic reactive distillation. *Topics in Catalysis*, **2006**. 40(1-4): p. 141-150.
- 537 55. Rabee, A.I., L.J. Durndell, N.E. Fouad, L. Frattini, M.A. Isaacs, A.F. Lee, G.A. Mekhemer, V.C.
538 dos Santos, K. Wilson, and M.I. Zaki, Citrate-mediated sol–gel synthesis of Al-substituted sulfated
539 zirconia *catalysts for α-pinene isomerization*. *Molecular Catalysis*, **2018**. 458: p. 206-212.
- 540 56. Xin, T., M. Ma, H. Zhang, J. Gu, S. Wang, M. Liu, and Q. Zhang, A facile approach for the
541 synthesis of magnetic separable Fe₃O₄@TiO₂, core–shell nanocomposites as highly recyclable
542 photocatalysts. *Applied Surface Science*, **2014**. 288: p. 51-59.
- 543 57. Naeimi, H. and Z.S. Nazifi, A highly efficient nano-Fe₃O₄ encapsulated-silica particles bearing
544 sulfonic acid groups as a solid acid catalyst for synthesis of 1, 8-dioxo-octahydroxanthene
545 derivatives. *Journal of Nanoparticle Research*, **2013**. 15(11): p. 2026.
- 546 58. Naeimi, H. and S. Mohamadabadi, Sulfonic acid-functionalized silica-coated magnetic
547 nanoparticles as an efficient reusable catalyst for the synthesis of 1-substituted 1 H-tetrazoles
548 under solvent-free conditions. *Dalton Transactions*, **2014**. 43(34): p. 12967-12973.
- 549 59. Gadamsetti, S., N. Mathangi, S. Hussain, V.K. Velisoju, and K.V. Chary, Vapor phase
550 *esterification of levulinic acid catalyzed by γ-Al₂O₃ supported molybdenum phosphate catalysts*.
551 *Molecular Catalysis*, **2018**.
- 552 60. Sheng, W., W. Wei, J. Li, X. Qi, G. Zuo, Q. Chen, X. Pan, and W. Dong, Amine-functionalized
553 magnetic mesoporous silica nanoparticles for DNA separation. *Applied Surface Science*, **2016**.
554 387: p. 1116-1124.
- 555 61. Sen, S., V. Govindarajan, C.J. Pelliccione, J. Wang, D.J. Miller, and E.V. Timofeeva, Surface
556 modification approach to TiO₂ nanofluids with high particle concentration, low viscosity, and
557 electrochemical activity. *ACS applied materials & interfaces*, **2015**. 7(37): p. 20538-20547.
- 558 62. Wang, J., P. Yang, M. Fan, W. Yu, X. Jing, M. Zhang, and X. Duan, Preparation and
559 characterization of novel magnetic ZrO₂/TiO₂/Fe₃O₄ solid superacid. *Materials letters*, **2007**.
560 61(11-12): p. 2235-2238.
- 561 63. Zhao, H., P. Jiang, Y. Dong, M. Huang, and B. Liu, A high-surface-area mesoporous sulfated
562 nano-titania solid superacid catalyst with exposed (101) facets for esterification: facile
563 preparation and catalytic performance. *New Journal of Chemistry*, **2014**. 38(9): p. 4541-4548.
- 564 64. Vieira, S.S., Z.M. Magriotis, N.A. Santos, A.A. Saczk, C.E. Hori, and P.A. Arroyo, Biodiesel
565 production by free fatty acid esterification using lanthanum (La³⁺) and HZSM-5 based catalysts.
566 *Bioresource technology*, **2013**. 133: p. 248-255.

- 567 65. Jamil, F., H. Ala'a, M.T.Z. Myint, M. Al-Hinai, L. Al-Haj, M. Baawain, M. Al-Abri, G. Kumar,
568 and A. Atabani, Biodiesel production by valorizing waste Phoenix dactylifera L. Kernel oil in the
569 presence of synthesized heterogeneous metallic oxide catalyst (Mn@ MgO-ZrO₂). Energy
570 Conversion and Management, **2018**. 155: p. 128-137.
- 571 66. Zhang, Z., H. Huang, X. Ma, G. Li, Y. Wang, G. Sun, Y. Teng, R. Yan, N. Zhang, and A. Li,
572 Production of diacylglycerols by esterification of oleic acid with glycerol catalyzed by diatomite
573 loaded SO₄²⁻/TiO₂. Journal of industrial and engineering chemistry, **2017**. 53: p. 307-316.
- 574